

Appendix A

Hall A HRS+Septum Optics Database Calibration

The pair of Hall A septum magnets were firstly used during small angle GDH [67] experiment in 2003. Due to an error of the installation, the left septum could not bend scattered particles with designed 6 degrees. So, first complete set of optics data was not taken until the Hall A hyper-nuclear [66] experiment started in December 2003. This chapter will describe the new C++ method used in the first HRS+Septum optics matrix optimization.

A.1 Introduction to HRS+Septum Optics

The optics of spectrometers is not traditional “optics” for mirrors and lens. It’s more like a matrix transforming variables from detector system to target system. In other words, optics is the software part of a spectrometer system which releases the full potential of the hardware.

A.1.1 Hall A coordinate conventions

In this section, a short overview of Hall A coordinate conventions is presented. For more details, they can be found in reference [106, 107]. All coordinate systems pre-

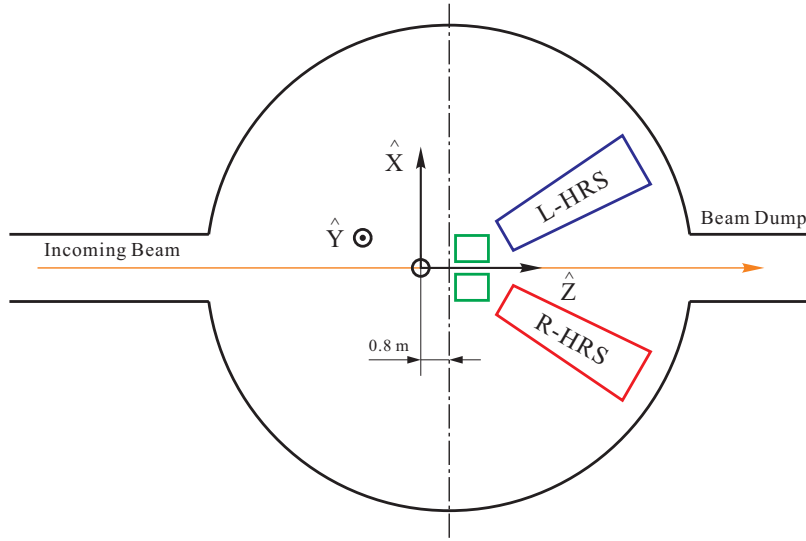


Figure A-1: Hall coordinate system (top view).

sented are Cartesian. Note that a reference to an angular coordinate in this section should be taken to refer to the tangent of the angle in question.

Hall Coordinate System (HCS)

The origin of the HCS is defined by the intersection of the electron beam and the vertical symmetry axis of the target system. As described in section 2.6, due to the installation of septum magnet the center is displaced by 0.8 m upstream from the geometry center of Hall A. Direction \hat{z} is along the beam line and points to the beam dump, \hat{y} is vertically up and \hat{x} is to the right facing the beam. See Figure A-1.

Target Coordinate System (TCS)

Each of the HRS is bundled with its own TCS. The central ray vertically passing through the center of sieve collimator¹ away from target defines the z_{tg} axis of the TCS for a given spectrometer. The \hat{y}_{tg} is pointing to the right and \hat{x}_{tg} is vertically down facing the central ray. See Figure A-2. In the ideal case where the spectrometer is pointing directly at the hall center and the sieve slit is perfectly centered on the

¹The sieve slit is placed before the entrance of septum magnet. It is used to replace normal single hole collimator for optics calibration purpose. The plot of sieve hole can be found in Figure A.2.2.

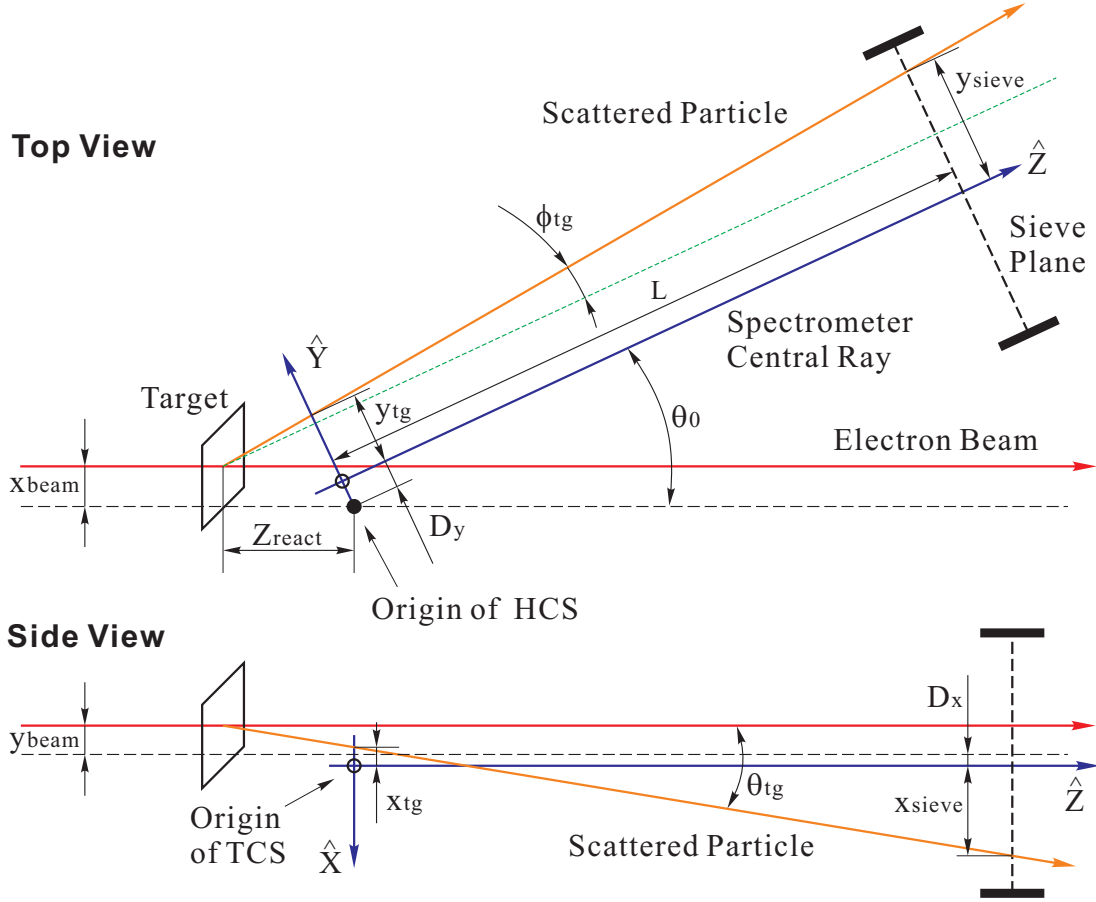


Figure A-2: Target coordinate system (top and side views).

spectrometer, the TCS has the same origin as HCS. However it typically deviates from HCS center by D_y and D_x in horizontal and vertical directions in TCS. And these shifts are given by survey. The distance of midpoint of the collimator from the TCS origin is defined to be a constant L for the spectrometer. The out-of-plane angle (θ_{tg}) and the in-plane angle (ϕ_{tg}) are given by dx_{sieve}/L and dy_{sieve}/L .

The TCS variables are used to calculate scattering angles and reaction points along the beam. Combined with beam variables (measured in the Hall coordinate system) the scattering angle and reaction point are given by

$$\theta_{scat} = \arccos\left(\frac{\cos(\theta_0) - \phi_{tg}\sin(\theta_0)}{\sqrt{1 + \theta_{tg}^2 + \phi_{tg}^2}}\right) \quad (A.1)$$

$$z_{react} = \frac{-(y_{tg} + D_y) + x_{beam}(\cos(\theta_0) - \phi_{tg}\sin(\theta_0))}{\cos(\theta_0)\phi_{tg} + \sin(\theta_0)}, \quad (A.2)$$

where θ_0 denotes the spectrometer central angle. The in-plane and out-of-plane angles can be determined using sieve hole positions:

$$\phi_{\text{tg}} = \frac{y_{\text{sieve}} + D_y - x_{\text{beam}}\cos(\theta_0) + z_{\text{react}}\sin(\theta_0)}{L - z_{\text{react}}\cos(\theta_0) - x_{\text{beam}}\sin(\theta_0)} \quad (\text{A.3})$$

$$\theta_{\text{tg}} = \frac{x_{\text{sieve}} + D_x + y_{\text{beam}}}{L - z_{\text{react}}\cos(\theta_0) - x_{\text{beam}}\sin(\theta_0)}. \quad (\text{A.4})$$

Furthermore,

$$y_{\text{tg}} = y_{\text{sieve}} - L\phi_{\text{tg}} \quad (\text{A.5})$$

$$x_{\text{tg}} = x_{\text{sieve}} - L\theta_{\text{tg}}. \quad (\text{A.6})$$

Detector Coordinate System (DCS)

The intersection of wire 184 of the VDC1 U1 plane and the perpendicular projection of wire 184 in the VDC1 V1 plane onto the VDC U1 plane defines the origin of the DCS. \hat{z} is perpendicular to the VDC planes pointing vertically up, \hat{x} is along the long symmetry axis of lower VDC pointing away from the hall center (See Figure A-3).

Using the trajectory intersection points p_n (where $n = \text{U1, V1, U2, V2}$) with the four VDC planes, the coordinates of the detector vertex can be calculated according to

$$\tan(\eta_1) = \frac{p_{\text{U2}} - p_{\text{U1}}}{d_2} \quad (\text{A.7})$$

$$\tan(\eta_2) = \frac{p_{\text{V2}} - p_{\text{V1}}}{d_2} \quad (\text{A.8})$$

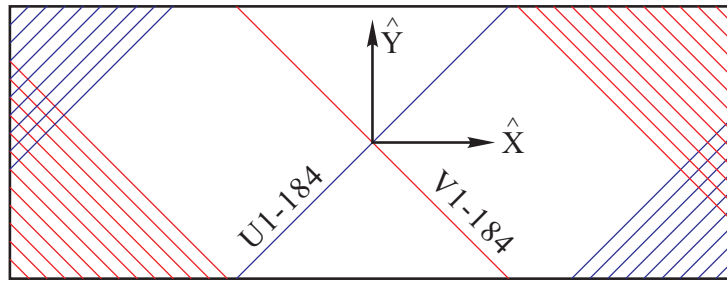
$$\theta_{\text{det}} = \frac{1}{\sqrt{2}}(\tan(\eta_1) + \tan(\eta_2)) \quad (\text{A.9})$$

$$\phi_{\text{det}} = \frac{1}{\sqrt{2}}(-\tan(\eta_1) + \tan(\eta_2)) \quad (\text{A.10})$$

$$x_{\text{det}} = \frac{1}{\sqrt{2}}(p_{\text{U1}} + p_{\text{V1}} - d_1\tan(\eta_2)) \quad (\text{A.11})$$

$$y_{\text{det}} = \frac{1}{\sqrt{2}}(-p_{\text{U1}} + p_{\text{V1}} - d_1\tan(\eta_2)). \quad (\text{A.12})$$

Top View



Side View

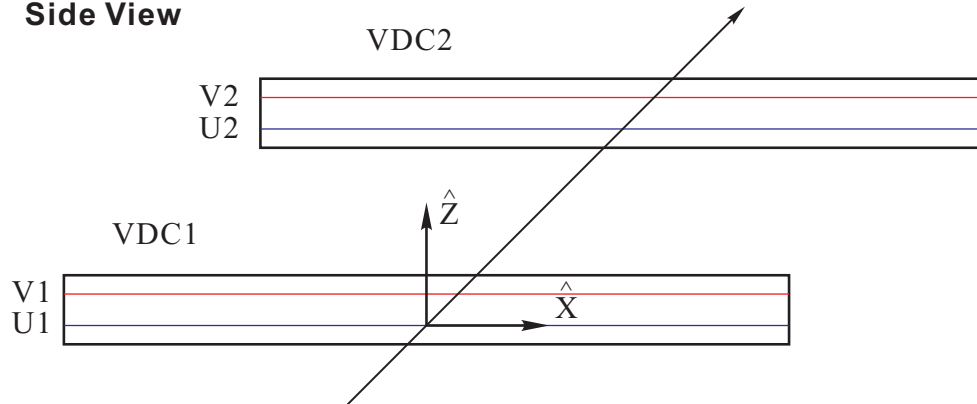


Figure A-3: Detector coordinate system (top and side views).

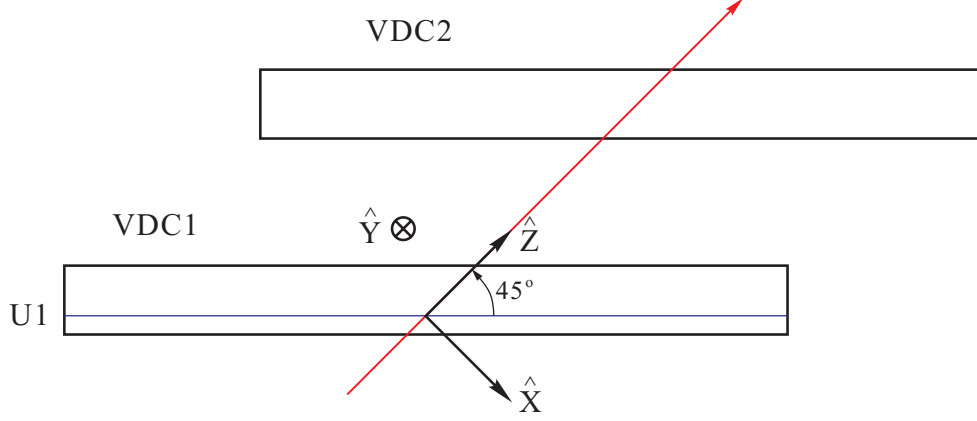


Figure A-4: Transport coordinate system.

Transport Coordinate System (TRCS)

The TRCS at the focal plane is generated by rotating the DCS clockwise around its y -axis by 45 degrees. It's typically used as a mediate stage from DCS to the FCS which will be described in next section. Ideally, the \hat{z} of the TRCS coincides with the central ray of the spectrometer. The transport coordinates can be expressed in terms of the detector coordinates by

$$\theta_{\text{tra}} = \frac{\theta_{\text{det}} + \tan(\rho_0)}{1 - \theta_{\text{det}} \tan(\rho_0)} \quad (\text{A.13})$$

$$\phi_{\text{tra}} = \frac{\phi_{\text{det}}}{\cos(\rho_0) - \theta_{\text{det}} \sin(\rho_0)} \quad (\text{A.14})$$

$$x_{\text{tra}} = x_{\text{det}} \cos(\rho_0) (1 + \theta_{\text{tra}} \tan(\rho_0)) \quad (\text{A.15})$$

$$y_{\text{tra}} = y_{\text{det}} + \sin(\rho_0) \phi_{\text{tra}} x_{\text{det}}, \quad (\text{A.16})$$

where $\rho_0 = -45^\circ$ is the rotation angle, see Figure A-4.

Transport Coordinate System (TRCS)

The focal plane coordinate system (FCS) chosen for the HRS analysis is a rotated coordinate system. Because of the focusing of HRS magnet system, particles from different scattering angles with same momentum will be focused at the focal plane. Therefore, the relative momentum to the central momentum of the spectrometer

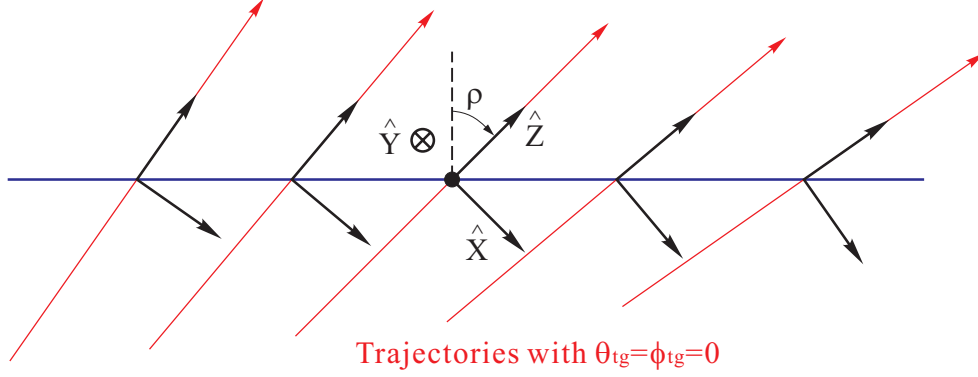


Figure A-5: Rotating focal plane system.

selected by magnet settings,

$$\delta = \frac{\Delta p}{p_0} = \frac{p - p_0}{p_0}, \quad (\text{A.17})$$

is approximately only a function of x_{tra} and p_0 in the form stands for the central momentum setting of HRS and Septum. And the FCS is obtained by rotating the DCS around its y -axis by an varying angle $\rho(x_{\text{tra}})$ to have the new \hat{z} axis parallel to the **local** central ray, which has scattering angle $\theta_{\text{tg}} = \phi_{\text{tg}} = 0$ for the corresponding δ at position x_{tra} . In this rotated coordinate system, the dispersive angle θ_{fp} is small for all points across the focal plane and approximately symmetric with $\theta_{\text{fp}} = 0$. Such symmetry will greatly simplify the further optics optimization.

With proper systematic offsets added, the coordinates of focal plane vertex can be written as follows:

$$x_{\text{fp}} = x_{\text{tra}} \quad (\text{A.18})$$

$$\tan(\rho) = \sum t_{i000} x_{\text{fp}}^i \quad (\text{A.19})$$

$$y_{\text{fp}} = y_{\text{tra}} - \sum y_{i000} x_{\text{fp}}^i \quad (\text{A.20})$$

$$\theta_{\text{fp}} = \frac{x_{\text{det}} + \tan(\rho)}{1 - \theta_{\text{det}} \tan(\rho)} \quad (\text{A.21})$$

$$\phi_{\text{fp}} = \frac{\phi_{\text{det}} - \sum p_{i000} x_{\text{fp}}^i}{\cos(\rho_0) - \theta_{\text{det}} \sin(\rho_0)}. \quad (\text{A.22})$$

The transfer is not unitary and we have x_{fp} equal to x_{tra} for simplicity.

A.1.2 Matrix Approach

For each event, two angular coordinates (θ_{det} and ϕ_{det}) and two spatial coordinates (x_{det} and y_{det}) are measured at the focal plane detectors. The position of the particle and the tangent of the angle made by its trajectory along the dispersive direction are given by x_{det} and θ_{det} , while y_{det} and ϕ_{det} give the position and tangent of the angle perpendicular to the dispersive direction. These variables are corrected for any detector offsets from the ideal central ray of the spectrometer to obtain the focal plane coordinates x_{fp} , θ_{fp} , y_{fp} and ϕ_{fp} . The focal plane observables are used to calculate θ , ϕ , y and δ at in the target system by matrix inversion.

The first order of such optics matrix can be expressed as,

$$\begin{pmatrix} \delta \\ \theta \\ y \\ \phi \end{pmatrix}_{\text{tg}} = \begin{pmatrix} \langle \delta|x \rangle & \langle \delta|\theta \rangle & 0 & 0 \\ \langle \theta|x \rangle & \langle \theta|\theta \rangle & 0 & 0 \\ 0 & 0 & \langle y|y \rangle & \langle y|\phi \rangle \\ 0 & 0 & \langle \phi|y \rangle & \langle \phi|\phi \rangle \end{pmatrix} \cdot \begin{pmatrix} x \\ \theta \\ y \\ \phi \end{pmatrix}_{\text{fp}}. \quad (\text{A.23})$$

The null tensor elements result from the mid-plane symmetry of the spectrometer.

In practice, the expansion of the focal plane coordinates is performed up to the fifth order. A set of tensors $D_{jkl}, T_{jkl}, Y_{jkl}$ and P_{jkl} links the focal plane coordinates to target coordinates according to [108]

$$\delta = \sum_{j,k,l} D_{jkl} \theta_{\text{fp}}^j y_{\text{fp}}^k \phi_{\text{fp}}^l \quad (\text{A.24})$$

$$\theta_{\text{tg}} = \sum_{j,k,l} T_{jkl} \theta_{\text{fp}}^j y_{\text{fp}}^k \phi_{\text{fp}}^l \quad (\text{A.25})$$

$$y_{\text{tg}} = \sum_{j,k,l} Y_{jkl} \theta_{\text{fp}}^j y_{\text{fp}}^k \phi_{\text{fp}}^l \quad (\text{A.26})$$

$$\phi_{\text{tg}} = \sum_{j,k,l} P_{jkl} \theta_{\text{fp}}^j y_{\text{fp}}^k \phi_{\text{fp}}^l, \quad (\text{A.27})$$

where the tensors $D_{jkl}, T_{jkl}, Y_{jkl}$ and P_{jkl} are polynomials in x_{fp} . For example,

$$D_{jkl} = \sum_{i=0}^m C_{ijkl}^D x_{\text{fp}}^i. \quad (\text{A.28})$$

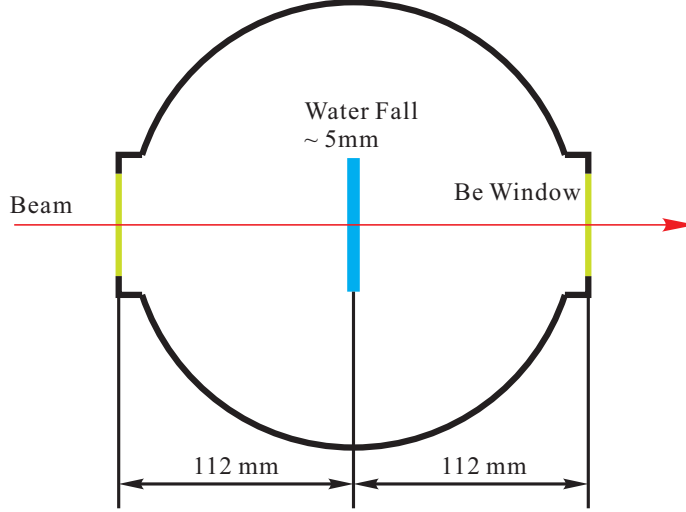


Figure A-6: Top section view of waterfall target.

A.2 Experimental and Optimization Procedure

A.2.1 Experiment

A full optimization of optics database requires sets of data with wide coverage on corresponding acceptance: δ in momentum, ϕ_{tg} and θ_{tg} in solid angle and y_{tg} for extended target. Other than reconstructed from detector variables the target variables' values in such experiments should also be obtained in other precise ways such as well known physics process: elastic scattering, nuclear excitation spectra or survey: target position, collimator sieve pattern. The ways are selected depending on which elements we want to optimize. Such kind of data were collected by performing the following series of calibration measurements.

- The first set of experiment were focused on angular and momentum calibration.
 1. A fixed energy 2037.2 MeV electron beam was incident on target. Two types of targets were used. One was typical 1 mm thick carbon and another one was a waterfall target build by INFN [109]. It contains a single waterfall with thickness around 5 mm and two 150 μm Be windows spaced by 224 mm as shown in Figure A-6.

2. Both HRS were positioned at 6 degrees. A pair of sieve slits with precisely drilled holes was used as collimators for the angular calibration, see Figure A.2.2.
 3. The central momentum of both spectrometers was adjusted so that it will deviate from the momentum of elastically scattered electrons at 6 degrees by a few percent. This deviation was varied from +4.5% to -4.5% in steps of 1.3%. At each step measurements were taken with both targets with and without sieve slits. We call such sweep a delta scan. The idea of delta scan is trying to minimize the changes applied to the beam energy. By only changing the magnetic settings of the spectrometers, we are still able to scan the whole momentum acceptance.
- The second set of experiment was used to optimize y elements.
 1. Three sets of carbon targets were used in this measurement. Except the single foil carbon target, the other two targets had two carbon foils spaced by 10 and 24 cm.
 2. A 3776.86 MeV electron beam was incident on target. Both spectrometers were set to collect inelastic scattering events, left arm at 1.96 GeV/ c and right arm at 1.57 GeV/ c .

During the calibration procedure, the raster was always turned off and the position of the beam on the target was kept within 100 μm away from the ideal beam line. As a result, the intersection point of the beam with the thin target foil provided a point target (to within the spectrometer resolution).

The following position and distances were then surveyed:

- the target position,
- the spectrometer central angles, and
- the position of the sieve slit center with respect to the spectrometer central axis.

A.2.2 Optimization Procedure and results

The major optics optimization procedure is illustrated in Figure A-7. The core program “Optimize++” was adopted from N. Liyanga’s code [107] for ESPACE [110] optics database. Some new features and scripts were integrated to comply the new Hall A C++ Analyzer [85].

The optimization begin with an initial optics database generated by magnetic field simulation using SNAKE [111]. The core of the optimization program is the TMinuit package of ROOT [86]. This package will vary the optics matrix parameters to minimize the variance σ^2 of reconstructed data from their actual values. And the variance is calculated in the following way:

$$\sigma^2(x) = \sum_{i=1}^m \sum_{j=1}^n (x_{i,j}^{\text{recon.}} - x_i^{\text{survey}})^2, \quad (\text{A.29})$$

where x can be any target variables, θ_{tg} , ϕ_{tg} , x_{tg} or δ , m is the total number of grid points measured in corresponding acceptance and n is number of events sampled for each point.

Sieve Pattern Reconstruction

The angular part of optics matrix was optimized firstly because the y_{tg} reconstruction and the elastic scattering momentum calculation are depending on the angles. The results from surveys were used to calculate the θ_{tg} and ϕ_{tg} of each hole.

The left figure shows the design of sieve slit, and the large holes are used to identify the orientation of the image at the focal plane. The right two plots show the improvement of the angular reconstruction from left HRS after optimization. As a result, we got θ_{tg} (out-of-plane angle) reconstructed with a resolution of 4 mrad FWHM and ϕ_{tg} (in-plane angle) with 1.5 mrad.

Momentum delta scan

The momentum calibration requires precise measurement of spectrometer central momentum. With the constants determined in reference [112] the central momentum of

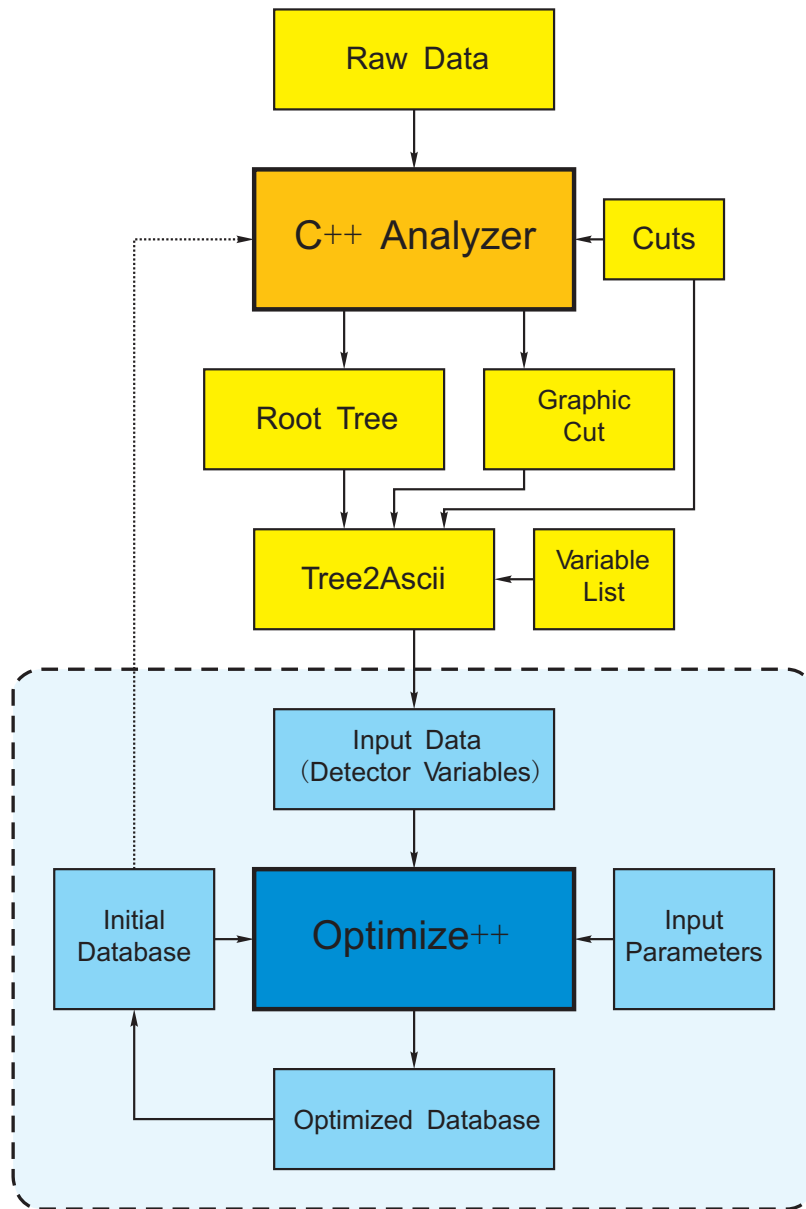


Figure A-7: Basic procedure for HRS+Septum optics optimization.

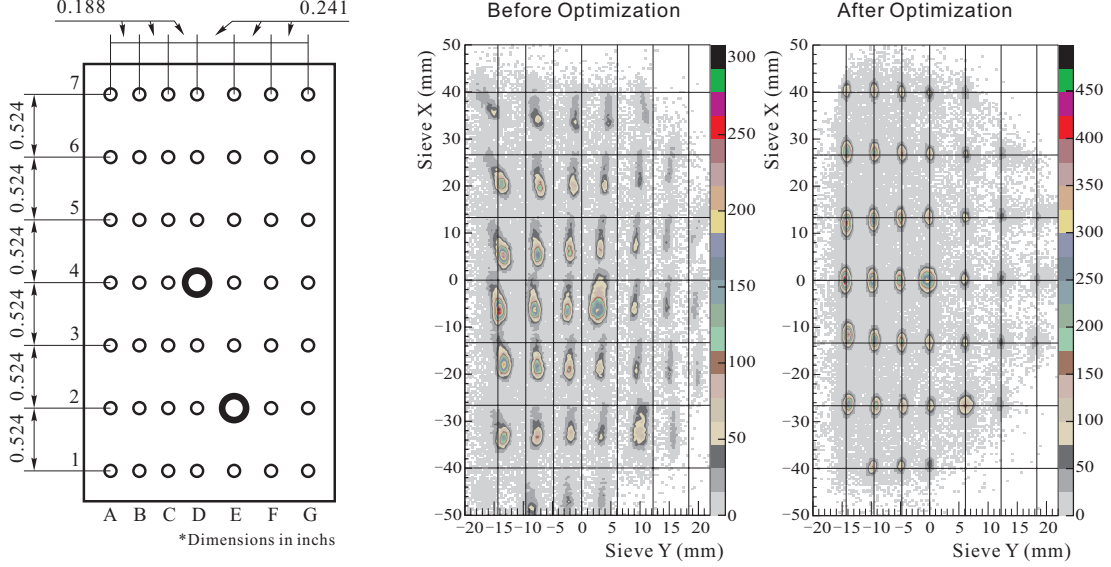


Figure A-8: Sieve Pattern Reconstruction.

each settings were calculated using magnet field readouts from dipoles.

One issue in the elastic peak reconstruction is the angular dependence. The elastically scattered electron has energy (omit the electron's mass):

$$p(M, \theta) = E' = \frac{E}{1 + E/M(1 - \cos(\theta))}, \quad (\text{A.30})$$

where E is incoming electron energy, M is target mass and θ is scattering angle. So the our solid angle acceptance, the elastic peak will be broadened by this dependence and the effect becomes larger for lighter target elements. To remove such effect, a new variable called dp_{kin} is defined by

$$dp_{\text{kin}} = dp - \frac{p(M, \theta_{\text{scat}}) - p(M, \theta_0)}{p_0}, \quad (\text{A.31})$$

where the scattering angle θ_{scat} is calculated using formula (A.1) and θ_0 is the central angle of spectrometer.

Figure A-9 shows the effect of this dp_{kin} correction in the water fall target elastic scattering. The hydrogen elastic peak after the correction can finally be clearly identified. Of course, this method is only valid for elastic scattering from known targets.

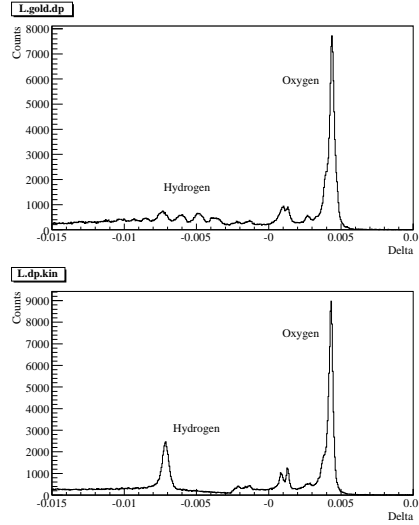


Figure A-9: dp_{kin} correction on elastic scattering from waterfall target.

Figure A-10 shows the results of a set of delta scan on Carbon target reconstructed using left HRS data.

The final relative momentum resolution is better than 2×10^{-4} .

Multi-foil targets

The y_{tg} optimization improved the transverse position resolution in target system to 2.5 mm FWHM, and it's corresponding to a 2.5 cm FWHM resolution of reaction point along beam in the 6 degrees configuration. The results are shown in Figure A-11.

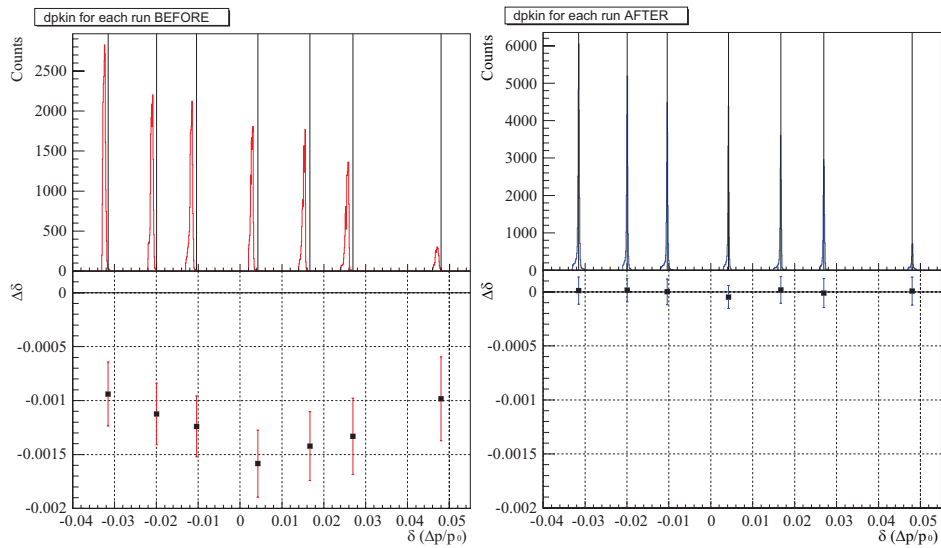


Figure A-10: Left HRS elastic peaks' reconstruction in a delta scan on Carbon target. The top plots show the absolute position of the peaks, the bottom plots show the deviation of reconstructed data from true values and the error bars show the resolution σ of those peaks.

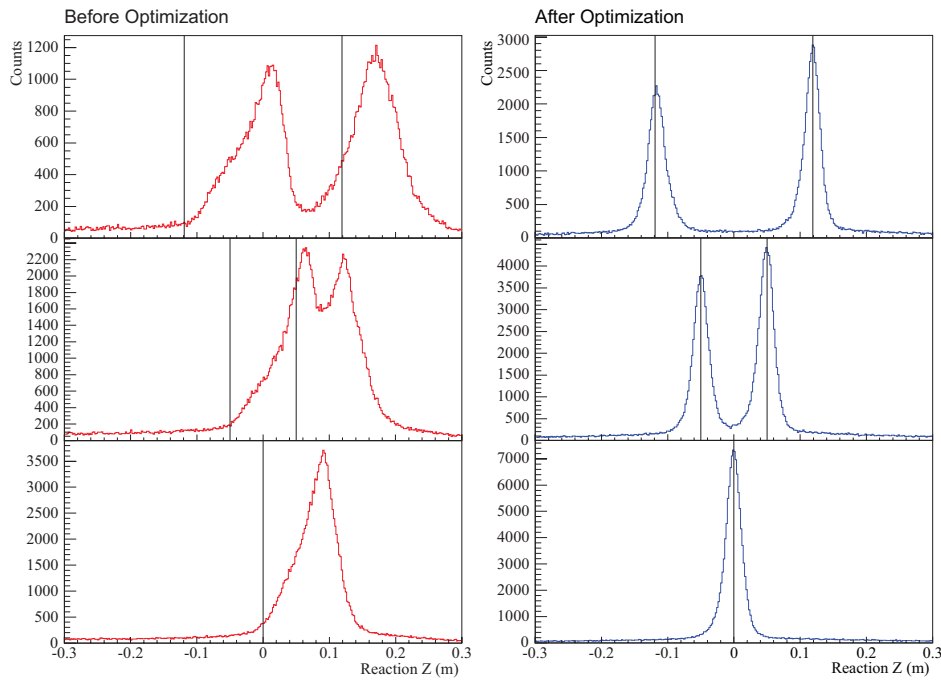


Figure A-11: Reaction positions reconstruction using multi-foil targets.

Bibliography

- [1] V. Petrov D. Diakonov and M. Polyakov. *Z. Phys.*, A359:305, 1997.
- [2] R. L. Jaffe and F. Wilczek. *Phys. Rev. Lett.*, 91:012002, 2003.
- [3] (CLAS) S. Stepanyan *et al.* *Phys. Rev. Lett.*, 91:250001, 2003.
- [4] (CLAS) S. Niccolai *et al.* *Phys. Rev. Lett.*, 97:032001, 2006.
- [5] (NA49) C. Alt *et al.* *Phys. Rev. Lett.*, 92:042003, 2004.
- [6] (STAR) H. Z. Huang. *Int. J. Mod. Phys.*, A21:825, 2006.
- [7] (HERMES) A. Airapetian *et al.* *Nucl. Phys.*, A755:379, 2005.
- [8] P. Reimer and B. Wojtsekhowski (spokespersons) *et al.* High Resolution Study of the 1540 Exotic State. *Jefferson Lab Proposal E04-012*, 2004.
- [9] R. L. Jaffe. *Phys. Rev.*, D15:267, 1977.
- [10] H. Hogaasen and P. Sorba. *Nucl. Phys.*, B145:119, 1978.
- [11] R. L. Jaffe. *Phys. Rev.*, D20:748, 1979.
- [12] R. L. Cool *et al.* *Phys. Rev. Lett.*, 17.
- [13] S. Mori *et al.* *Phys. Rev.*, 185:1687, 1969.
- [14] (Particle Data Group) T. G. Trippe *et al.* *Rev. Mod. Phys.*, 48:S1, 1976.
- [15] T. H. Skyrme. *Proc. Soc. Lond.*, A260:1975, 1961.

- [16] T. H. Skyrme. *Nucl. Phys.*, 31:556, 1962.
- [17] E. Witten. *Nucl. Phys.*, B223:433, 1983.
- [18] E. Witten. *Nucl. Phys.*, B223:422, 1983.
- [19] E. Guadagnini. *Nucl. Phys.*, B236:35, 1984.
- [20] D. Diakonov and V. Petrov. *talks at the ITEP Winter School*, 1984.
- [21] A. Manohar. *Nucl. Phys.*, B248:19, 1984.
- [22] M. Chemtob. *Nucl. Phys.*, B256:600, 1985.
- [23] M. Praszalowicz. *Proc. of the Workshop Skyrmions and Anomalies, Krakow, Poland, World Scientific*, page 112, 1987.
- [24] (LEPS) T. Nakano *et al.* *Phys. Rev. Lett.*, 91:012002, 2003.
- [25] K. H. Hicks. *Prog. Part. Nucl. Phys.*, 55:647, 2005.
- [26] V. D. Burkert. *Int. J. Mod. Phys.*, A21:1764, 2006.
- [27] R. A. Schumacher. nucl-ex/0512042. 2005.
- [28] (DIANA) V. V. Barmin *et al.* *Phys. Atom, Nuclei*, 66:1715, 2003.
- [29] (SAPHIR) J. Barth *et al.* *Phys. Lett.*, B572:127, 2003.
- [30] K. Hicks. *Int. J. Mod. Phys.*, A20:219, 2006.
- [31] (CLAS) M. Battaglieri *et al.* *Phys. Rev. Lett.*, 96:042001, 2006.
- [32] W. Dunwoodie. *JLab Users Group Meeting*, 2006.
- [33] A. E. Asratyan *et al.* *Phys. Atom. Nucl.*, 67:682, 2004.
- [34] The ZEUS collaboration. *Phys. Lett.*, B591:7, 2004.
- [35] (COSY-TOF) M. Abdel-Barv *et al.* *Phys. Lett.*, B595:127, 2004.

- [36] A. Hosaka S. I. Nam and H. C. Kim. *Phys. Lett.*, B633:483, 2006.
- [37] (BES) J. Z. Bai *et al.* *Phys. Rev.*, D70:012004, 2004.
- [38] The Belle Collaboration. hep-ex/0409010.
- [39] (ALEPH) S. Schael *et al.* *Phys. Lett.*, B599:1, 2004.
- [40] (HERA-B) I. Abt. *et al.* *Phys. Rev. Lett.*, 93:212003, 2003.
- [41] (SPHINX) Yu M. Antipov *et al.* *Eur. Phys. J.*, A21:455, 2004.
- [42] (HyperCP) M. J. Longo *et al.* *Phys. Rev.*, D70:111101, 2004.
- [43] (CDF) D. O. Litvintsev *et al.* hep-ex/0410024.
- [44] M. V. Polyakov I. I. Strakovsky R. A. Arndt, Y. I. Azimov and R. L. Workman. *Phys. Rev.*, C69:035208, 2004.
- [45] S. Nussinov. hep-ph/0307357.
- [46] R. A. Arndt *et al.* *Phys. Rev.*, C68:042001, 2003.
- [47] J. Haidenbauer and G. Krein. *Phys. Rev.*, C68:052201, 2003.
- [48] W. R. Gibbs. *Phys. Rev.*, C70:045208, 2004.
- [49] T. Bowen *et al.* *Phys. Rev.*, D2:2599, 1970.
- [50] I. I. Strakovsky R. L. Workman Y. I. Azimov, R. A. Arndt and K. Goeke. *Eur. Phys. J.*, A26:79, 2005.
- [51] S. Capstick *et al.* *Phys. Lett.*, B570:185, 2003.
- [52] H. Gao and B. Q. Ma. *Mod. Phys. Lett.*, A14:2313, 1999.
- [53] (Particle Data Group) K. Hagiwara *et al.* *Phys. Rev.*, D66:1, 2002.
- [54] (CLAS) V. Kubarovsky *et al.* *Phys. Rev. Lett.*, 97:102001, 2006.

- [55] P. Brindza *et al.* Superconducting Septum Magnet Design for Jefferson Lab Hall A. *IEEE Transactions on applied superconductivity*, 11:1594, March 2001.
- [56] P. Chevtsov *et al.* Synchrotron Light Interferometer at Jefferson Lab. *Proceedings of the 2003 Particle Accelerator Conference*, 2003.
- [57] T. Mitsuhashi. Beam Profile Measurement by SR Interferometers. *Proceedings of the Joint U.S.-CERN-Japan-Russia School on Particle Accelerators, Montreux, Switzerland*, 1998.
- [58] M. G. Minty and F. Zimmerman. Measurement and Control of Charged Particle Beams, Springer-Verlag, Berlin. page 163, 2003.
- [59] J. Alcorn *et al.* Basic instrumentation for Hall A at Jefferson Lab. *Nucl. Instr. and Meth*, A522:294, 2004.
- [60] K. Unser. *IEEE Trans. Nucl. Sci.*, NS28:2344, 1981.
- [61] W. Barry *et al.* Beam Position Measurement in the CEBAF Recirculating Linacs by use of Pseudorandom Pulse Sequences, JLab-TN-90-246. 1990.
- [62] W. Barry *et al.* Basic Noise Considerations for CEBAF Beam Position Monitors, JLab-TN-91-087. 1991.
- [63] R. A. Lindgren. A CDR for a new Scattering Chamber for Hall A. 2001.
- [64] <http://halloweb.jlab.org/equipment/BigBite/>.
- [65] http://halloweb.jlab.org/equipment/targets/cryotargets/Halla_tgt.html.
- [66] F. Garibaldi *et al.* High Resolution 1p-Shell Hypernuclear Spectroscopy. *JLab Experiment E94-107*, 1994.
- [67] A. Deur J. P. Chen and F. Garibaldi (spokespersons) *et al.* The GDH Sum Rule, the Spin Structure of ^3He and the Neutron using Nearly Real Photons. *Jefferson Lab Experiment E97-110*, 1997.

- [68] R. Michaels (spokesperson) *et al.* Parity Experiment in HALL A, <http://halloweb.jlab.org/parity/>.
- [69] W. Bertozzi *et al.* *Nucl. Instr. and Meth.*, 191:957, 1977.
- [70] K. G. Fissum *et al.* Vertical Drift Chambers for the Hall A High Resolution Spectrometers at Jefferson Lab. *Nucl. Instr. and Meth.*, A 474:108, 2001.
- [71] B. Wojtsekhowski *et al.* High Performance Threshold Aerogel Counters. *Nucl. Instr. and Meth.*
- [72] P. A. Čerenkov. *Phys. Rev.*, 52:378, 1937.
- [73] E. Fermi. *Phys. Rev.*, 57:485, 1940.
- [74] R. Perrino *et al.* *Nucl. Instr. and Meth.*, A457:571, 2001.
- [75] L. Lagamda *et al.* *Nucl. Instr. and Meth.*, A471:325, 2001.
- [76] R. Iommi *et al.* Test and Development of a Cherenkov diffusion detector prototype using Airglass aerogel at TJNAF, JLab-TN-00-010. 2000.
- [77] ALICE Collaboration. Technical Design Report of the High Momentum Particle Identification Detector, CERN/LHCC98-19, Alice TDR 1. 1998.
- [78] F. Garibaldi (spokesperson) *et al.* The Hall A RICH Detector. *Hall A Status Report 2001*, 2001.
- [79] B. Reitz. TOSP for the Hall A RICH Detector. 2003.
- [80] DuPont™ Tedlar®PVF Film. <http://www.dupont.com/tedlar/>.
- [81] Hall A Operations Manual. 2000.
- [82] A. Deur. TJNAF E94-010 Technical Note E94010-TN-03.
- [83] Jefferson Lab Data Acquisition Group. The CODA Data Acquisition System, <http://coda.jlab.org>.

- [84] Experimental Physics and Industrial Control System,
<http://www.aps.anl.gov/epics>.
- [85] <http://halloweb.jlab.org/root/index.html>.
- [86] <http://root.cern.ch>.
- [87] C. L. Woody *et al.* *J. Phys. G: Nucl. Phys.*, 33:275, 2006.
- [88] L. Zhu. Particle Identification with Aerogel Cherenkov Detector A1/A2. *Write-up for Hall A Data Analysis Workshop 2001*, Dec. 2001.
- [89] P. E. Ulmer. *Ph.D. thesis, MIT*, 1998.
- [90] D. V. Jordan. *Ph.D. thesis, MIT*, 1994.
- [91] L. Weinstein. *Ph.D. thesis, MIT*, 1988.
- [92] G. Cowan *et al.* *Phys. Lett.*, B592:275, 2003.
- [93] P. Markowitz (spokesperson) *et al.* Electroproduction of Kaons up to $Q^2 = 3(\text{GeV}/c)^2$. *Jefferson Lab Proposal E98-108*, 1998.
- [94] W. M. Yao *et al.* *J. Phys. G: Nucl. Phys.*, 33:31, 2006.
- [95] J. J. Sakurai. *Modern Quantum Mechanics*. page 421.
- [96] J. D. Jackson *et al.* *J. Phys. G: Nucl. Phys.*, 33:321, 2006.
- [97] D. C. Fries *et al.* *Nucl. Phys.*, B143:408, 1978.
- [98] D. P. Barber *et al.* *Z. Phys.*, C12:1, 1982.
- [99] G. J. Feldman and R. D. Cousins. Unified Approach to the Classical Statistical Analysis of Small Signals. *Phys. Rev.*, D7:57, 1998.
- [100] J. Neyman. *Trans. R. Soc. London*, A236:333, 1937.
- [101] F. James *et al.*

- [102] S. Baker and R. D. Cousins. *Nucl. Instr. and Meth.*, A221:437, 1984.
- [103] W. A. Rolke *et al.* *Nucl. Instr. and Meth.*, A551:493, 2005.
- [104] R. D. Cousins and Highland. *Nucl. Instr. and Meth.*, A320:331, 1992.
- [105] G. J. Feldman. <http://conferences.fnal.gov/cl2k/copies/feldman2.pdf>.
- [106] ESPACE Users Guide. 1997.
- [107] N. Liyanaga. Optics calibration of the Hall A High Resolution Spectrometers using the New C++ Optimizer, JLab-TN-02-012. 2002.
- [108] M. Berz *et al.* Spectrometer Constant Determination for the Hall A HRS Pair. *Nucl. Instr. and Meth.*, A258:402, 1987.
- [109] Istituto Nazionale di Fisica Nucleare, Rome, Italy, <http://www.infn.it/indexen.php>.
- [110] Event Scanning Program for Hall A Collaboration Experiments, <http://hallaweb.jlab.org/espace/index.html>.
- [111] <http://hallaweb.jlab.org/news/minutes/tranferfuncs.html>.
- [112] N. Liyanaga. Spectrometer constant determination for the Hall A HRS Pair, JLab-TN-01-049. 2001.